05

Ultrafast photo-induced phenomena in magnetic semiconductor EuO

© P.A. Usachev, L.A. Shelukhin, V.V. Pavlov

Ioffe Institute,
St. Petersburg, Russia

E-mail: Usachev@mail.ioffe.ru

Received March 6, 2025
Revised March 6, 2025
Accepted May 5, 2025

The results of a study on ultrafast photo-induced phenomena in the intrinsic magnetic semiconductor EuO, using the two-color optical pump-probe technique, are presented. Experimental data demonstrate photo-induced magnetization precession in the temperature range below the Curie temperature, excited by circularly polarized light. Numerical estimates have been performed for two possible mechanisms of optical excitation of the magnetization precession, related to the optical orientation effect and the inverse Faraday effect. Based on theoretical modeling, it is shown that the optical orientation of spin through the electron transition $4f^7 5d^0 \rightarrow 4f^6 5d^1$ is the triggering mechanism of the magnetization precession. Photoexcitation of EuO by light with photon energy greater than the band gap leads to the formation of magnetic polarons due to the strong exchange interaction of the $5d^1$1 electron spin with the spins of $4f$ electrons. The dynamics of magnetic polarons in the time range from a few picoseconds to microseconds has been revealed. At temperatures slightly above the Curie temperature, a record high value of the magnetic moment of polarons has been established.

Keywords: photo-induced magneto-optical phenomena, optical orientation effect, inverse Faraday effect, magnetization dynamics, magnetic polarons, ferromagnetic semiconductor.

DOI: 10.61011/PSS.2025.07.61889.26HH-25

1. Introduction

The ability to control the magnetic state of materials using light is of fundamental interest and is also very important for practical applications in the field of ultrafast recording and processing of information. Ultrafast optical manipulation of magnetization is one of the most promising research directions in solid-state physics and spintronics [1,2]. Various physical mechanisms that may be responsible for the optical effect on the spin system of solids are discussed in the literature. In Ref. [3], it was theoretically predicted that light can act as an effective magnetic field due to the inverse Faraday effect (IFE). On the femtosecond time scale, the IFE has been experimentally demonstrated in various classes of materials [4,5]. The IFE arises from the nonlinear interaction of light with matter [6]. The microscopic description of IFE involves either spin sublevel splitting through the optical Stark effect, or as the stimulated Raman scattering on magnons, see [7,8]. Other mechanisms of optical control of magnetization are based on the laser-induced changes in the magnetic anisotropy [9,10], or through ultrafast heating of the magnetic system by short laser pulses [11]. The optical orientation effect (OOE) is well known in the field of semiconductor optics [12]. This effect was first demonstrated as the spatial orientation of atoms induced by circularly polarized light [13]. In solids, OOE determines the transfer of angular momentum from circularly polarized photons to electrons, whose spin orientation arises as a result of spin-orbit interaction. The transfer of the angular momentum from optically excited electrons to collective magnetization can give rise to a light-induced magnetic response. For example, magnetization precession driven by optical excitation was demonstrated in the diluted magnetic semiconductor (Ga,Mn)As [14]. In the case of intrinsic magnetic semiconductors, the exchange interaction between spin-polarized photo-excited carriers and local magnetic moments may significantly enhance the magnetic response to photoexcitation. Both effects, IFE and OOE, arise from the interaction of circularly polarized light with the spin system. Therefore, establishing the key mechanism of the optically excited precession is crucial. This research aims to unravel the dynamics of magnetic states in the magnetic semiconductor EuO driven by sub-picosecond laser pulses. Here, we provide a mini-review of our studies on photo-induced phenomena in EuO, focusing on the excitation of magnetization precession and giant magnetic polarons (MP) with a large magnetic moment.

Europium oxide EuO is a representative of europium chalcogenides (EuX) group, which are binary compounds of europium (Eu) and chalcogens (X = O, S, Se and Te). Europium chalcogenides EuX possess a number of unique physical properties determined by their electronic structure. Europium oxide EuO is a magnetic semiconductor with the classic Heisenberg ferromagnetic ordering. EuO crystallizes in a cubic syngony with a NaCl-type structure and point group $m3m$, $a = 5.145$ A, $Z = 4$ (see Figure 1, a). The valence and conduction bands of EuO are primarily formed by the $4f$- and $5d$-states of Eu^{2+} ions, respectively (see Figure 1, b). Below the Curie temperature of $T_C = 69.8$ K a magnetic order forms in the system of highly localized $4f^7$

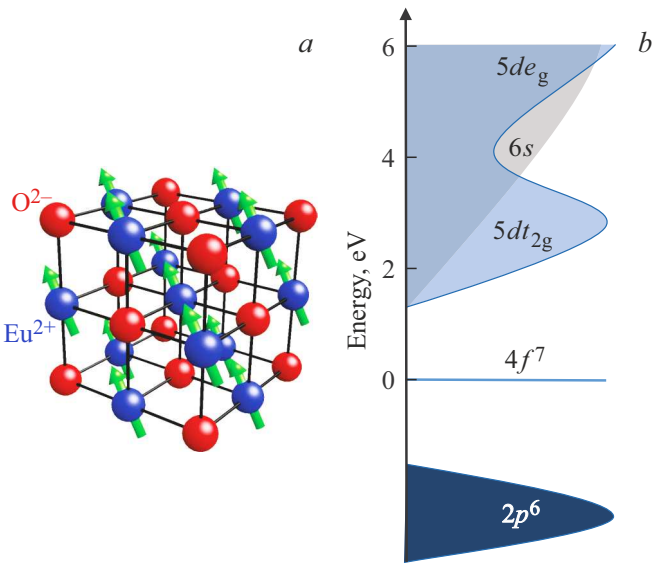

Figure 1. (*a*) Crystallographic, magnetic and (*b*) electronic structure of the EuO crystal.

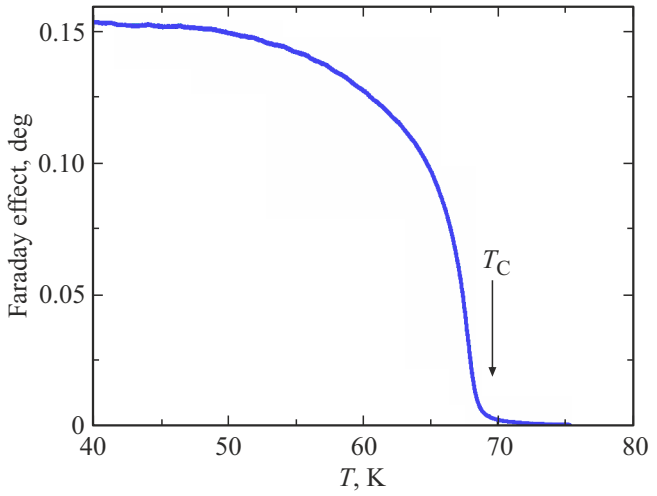

Figure 2. Temperature dependence of the Faraday effect in EuO (from Ref. [15]).

electrons of the Eu^{2+} ions with a spin $S = 7/2$. The Faraday effect temperature dependence for our EuO film (from Ref. [15]) is presented in Figure 2. These measurements, performed in a tilted geometry with an in-plane magnetic field, verify the easy-plane anisotropy reported for such films in Ref [16]. The data thus confirm the easy-plane anisotropy in our samples and directly demonstrate the formation of the magnetic order. EuO exhibits a strong coupling between its electronic and magnetic properties; for instance, its electrical transport characteristics change significantly upon the emergence of magnetic order. Giant linear and quadratic magneto-optical Kerr effects have been observed in EuO films [16,17] as a direct consequence of its unique electronic structure. This combination of properties makes EuO an exceptional material for potential practical applications. Notable examples include the optical control of its magnetic order parameter [18–20]. In spintronics, EuO is considered a promising multiferroic material [21] and can serve as a ferromagnetic component for spin-transistor elements [22].

2. Samples and Experimental Methods

The studied EuO films were $l = 100-200$ nm thick, epitaxially grown on yttria-stabilized zirconia (YSZ) substrates and protected by a transparent SiO_{2-x} capping layer [15,16,20]. The lattice parameter of substrate YSZ (5.147 Å) is close to the lattice parameter of bulk crystal of EuO (5.145 Å). The EuO film growth process was monitored using standard techniques, which confirmed the high crystalline quality of the samples. This quality control ensures that the physical properties of the resulting films closely match those of bulk EuO. The magnetic properties of EuO films were studied using SQUID magnetometry [15,16,20], and by measurement of the magneto-optical Kerr effect [16]. The data confirm that the key magnetic parameters of the bulk material (The Curie temperature T_C and saturation magnetization M_s), are retained in the films.

Figure 3 shows a schematic of the experimental setup for detecting photo-induced magnetization precession via the Faraday effect. A femtosecond laser with a photon energy of 1.19 eV generates pulses with a duration of $t_p = 190$ fs and repetition rate of 5 kHz. A beam splitter separates the light into a pump beam and a probe beam. The pump beam passes through a nonlinear β-BaB_2O_4 (BBO) crystal, where its photon energy is doubled to $\hbar\omega = 2.38$ eV via second harmonic generation. The pump power density is $j_p = 5\,\mathrm{mJ/cm^2}$. The resulting green pump beam is directed through a modulator. For studies of photo-induced magnetization precession, an electro-optical modulator (EOM) is used to switch the pump pulse polarization between right- and left-handed circular. For investigations of magnetic polarons via the photo-induced Faraday effect, a mechanical chopper is employed instead. In both configurations, the modulation is synchronized with the laser repetition rate. The probe beam detects the pump-induced change in the Faraday effect after both beams overlap on the sample spot. The probe beam is at normal incidence (0 deg), while the pump beam is incident at an angle of 20 deg. After passing through the sample, the probe beam is analyzed by a balanced photodetector. The resulting electrical signal is measured by a lock-in amplifier, providing a sensitivity to the polarization rotation angle of $\sim 10^{-7}$ rad. Thus, by modulating the polarization or intensity of the pump, this method allows us to extract the weak photo-induced signal of interest from the strong, non-modulated background of the Faraday effect.

The EuO sample was mounted in an optical cryostat, allowing for temperature control across the 10–300 K range.

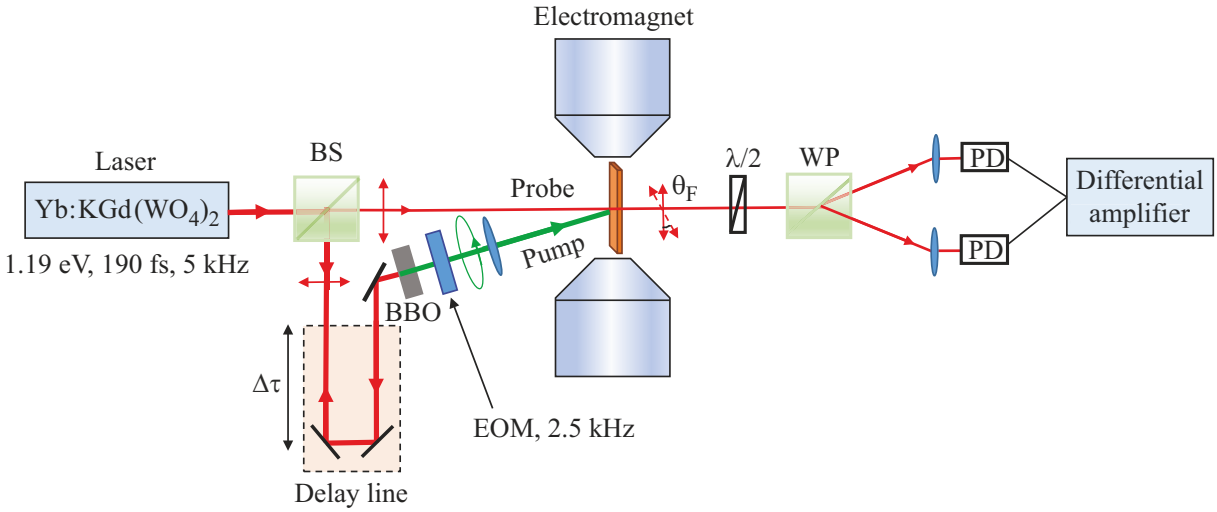

Figure 3. Experimental setup for two-color pump-probe measurements. BS — beam splitter, BBO — non-linear crystal of barium boron oxide, EOM — electrooptical modulator, $\lambda/2$ — half-wave plate, WP — Wollaston prism, PD — photodiode.

External magnetic field with induction of $B = \pm 600\,\text{mT}$ can be applied parallel or perpendicular to the sample plane. The time interval between the pump and probe pulses was varied using an opto-mechanical delay line. The measured value in this experiment is the light polarization plane rotation angle due to the Faraday effect Θ_F depending on the time delay $\Delta\tau$. From this value, the photo-induced magnetization M_z can be derived using the static Faraday effect data for EuO. For EuO films with easy-plane magnetic anisotropy, the rotation angle of the polarization plane in the Faraday geometry ($\mathbf{B} \parallel \mathbf{k} \parallel \mathbf{z}$, where $\mathbf{k}$ — wave vector of light, $\mathbf{z}$ — vector of normal line to the sample plane) linearly depends on the applied magnetic field up to the saturation field $B_s = 2.4\,\text{T}$. The magnetization also increases linearly with the magnetic field, having a slope of M_s/B_s. Therefore, the measured photo-induced polarization rotation can be expressed as the normalized photo-induced magnetization M_z/M_s.

3. Photoinduced precession of magnetization

This section considers the precession of photoinduced magnetization in EuO, excited by a circularly polarized light. In this experiment the sample was maintained at temperature that is much below T_C, and the external magnetic field was applied along the sample plane.

The light-induced excitation of magnetization precession in the EuO film is shown in Figure 4, *a*. In contrast to Ref. [20], where magnetization precession was excited by pulses with fixed circular polarization, the present work measures the photo-induced magnetization change by modulating the pump polarization between right- and left-handed. Since the total pump intensity remains constant, this method completely eliminates contributions from thermal changes in magnetization, isolating the signal that originates solely from the pump polarization reversal. The dots in Figure 4, *a* show the normalized magnetization measured via the photoinduced Faraday effect in a 200 mT magnetic field. The relationship between the magnetization precession frequency and the external magnetic field is presented in Figure 4, *b*. The observed dependence is in excellent agreement with the data reported in [20]. A decrease in the precession frequency is observed between 0–60 mT, followed by an almost linear increase with the applied field up to 200–600 mT. Given that thermal effects are negligible, the precession must be driven by an effective magnetic field. Its origin lies in the nonlinear interaction of circularly polarized light with matter, specifically either the inverse Faraday effect or the optical orientation effect, which is capable of producing an effective magnetic Weiss field.

To quantify the contributions of these potential mechanisms to the precession onset, theoretical modeling of the magnetization excitation via IFE and OOE is required. The magnetic moment $\mathbf{M}$ of the valence-band $4f$-electrons exhibits precession in response to internal or external magnetic fields, governed by the Landau-Lifshitz equation [23,24]:

$$\frac{d\mathbf{M}}{dt} = \gamma[\mathbf{M} \times \mathbf{H}_{\text{eff}}] - \alpha \frac{\gamma}{M_s} \left(\mathbf{M} \times [\mathbf{M} \times \mathbf{H}_{\text{eff}}]\right), \qquad (1)$$

here γ represents the gyromagnetic ratio, α is the dimensionless damping constant for the relaxation of magnetization $\mathbf{M}$, and $\mathbf{H}_{\text{eff}}$ is the effective magnetic field. This field, given by equation (1), comprises a vector sum of several terms:

$$\mathbf{H}_{\text{eff}} = \mathbf{H}_0 + \mathbf{H}_{\text{anis}} + \mathbf{H}_{\text{dem}}, \qquad (2)$$

where $\mathbf{H}_0$ is the external magnetic field, $\mathbf{H}_{\text{anis}}$ is the anisotropy field, and $\mathbf{H}_{\text{dem}}$ is the demagnetization field.

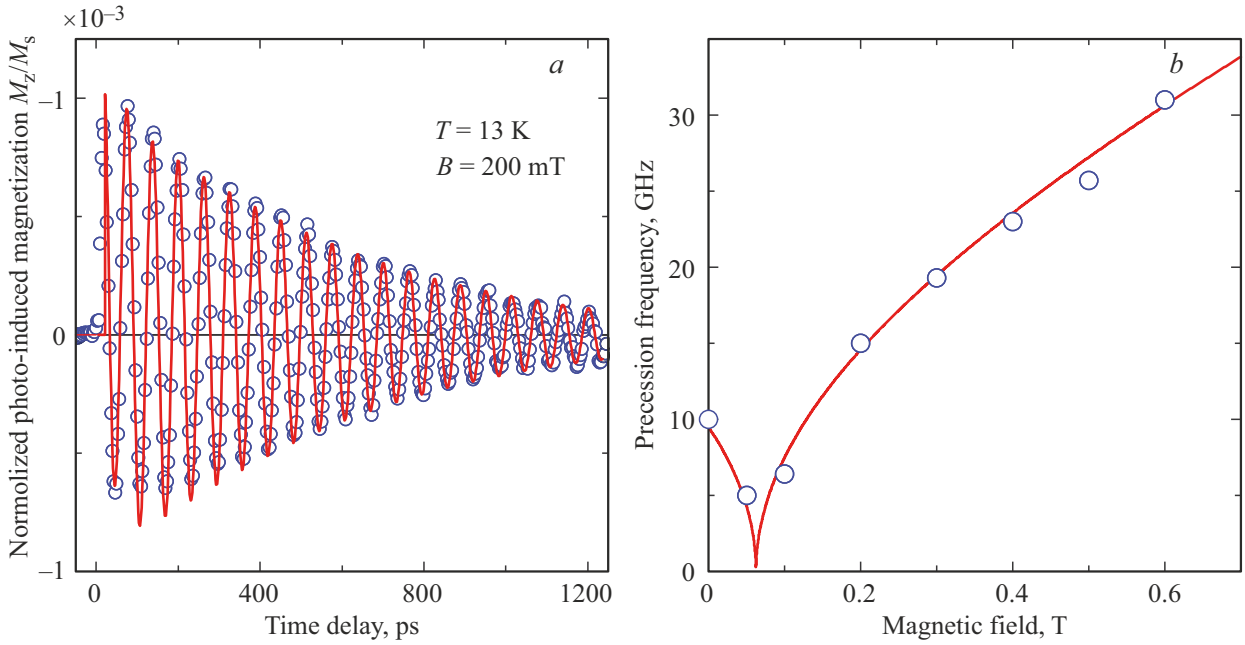

Figure 4. (*a*) Normalized photo-induced magnetization in EuO film. Blue dots represent the experimental data, and the red line is the calculation according to equation (1). (*b*) Magnetization precession frequency, $\Omega/2\pi$, as a function of the external magnetic field. Blue dots represent the experimental data, and the red line is the calculation according to equation (3).

The precession frequency is given by the solution of equation (1) [25]:

$$\Omega = \frac{\gamma}{M_s \sin\theta}\sqrt{F_{\theta\theta}F_{\varphi\varphi} - F_{\theta\varphi}^2}, \tag{3}$$

where $F_{\theta\theta}$, $F_{\varphi\varphi}$ and $F_{\theta\varphi}$ denote the second derivatives of the anisotropic free energy density F relative to the spherical coordinates θ and φ of the magnetization vector. The necessary anisotropy constants for estimating the EuO free energy are available in the literature, namely $K_1/M_s \sim -247.5$ Oe and $K_2/M_s \sim 82$ Oe at $T = 4.2$ K [26]. The excellent agreement in Figure 4, *b* between the experimental data (dots) and theoretical calculations (line) is consistent with the results reported in [20].

Numerical assessment of the IFE requires the computation of the effective magnetic field $\mathbf{H}^{\mathrm{IFE}}$, which is parametrically generated by an optical wave through a two-photon process [27]. The expression for this field is given by [28]:

$$\mathbf{H}^{\mathrm{IFE}} = -i\,\frac{\epsilon_0}{\mu_0}\frac{G}{M_s}\,\mathrm{Im}\left[\mathbf{E}\times\mathbf{E}^*\right], \tag{4}$$

where G is the magnitude of the gyration vector, and $\mathbf{E}$ is the optical electric field. G in EuO can be evaluated using the reported magneto-optical Kerr effect parameters $\theta_K + i\epsilon_K \sim -3 + i$ deg at $\hbar\omega = 2.38$ eV and $T = 10$ K [29] together with the optical dielectric constant $\epsilon_1 + i\epsilon_2 \sim 2.5 + i1.1$ from [30,31]. The pump-induced magnetic field $\mathbf{H}^{\mathrm{IFE}}$ is confined to the laser pulse duration [3,6,32] and decays rapidly thereafter. The laser pump pulse has a Gaussian profile:

$$I(t) = \frac{I_0}{\varrho\sqrt{2\pi}}\exp\left(-\frac{t^2}{2\varrho^2}\right), \tag{5}$$

with $\varrho = t_p/\sqrt{\ln 256}$ representing the RMS temporal width of the pulse. Importantly, the light-induced magnetic field $H^{\mathrm{IFE}} \propto \pm I(\sigma^{\pm})$ changes sign according to the helicity of the pump pulse $\sigma^{\pm}$.

Let us now examine in more detail the mechanism of magnetization precession onset via IFE under pulsed laser pumping. Under subpicosecond optical excitation, the primary source of the $\mathbf{H}^{\mathrm{IFE}}$ field is the diamagnetic term in the IFE [7]. Initially in-plane, the magnetization cannot react instantaneously to the ultrafast external excitation [8]. Therefore, the IFE estimate from equation (4), based on the gyration vector magnitude G, represents an upper boundary as it includes both diamagnetic and magnetization-dependent contributions. The optical excitation drives the initially in-plane saturation magnetization $\mathbf{M}_s$ into precession at frequency Ω. Figure 5, *b* shows a schematic representation of the magnetization precession onset in EuO. The precession occurs around the effective magnetic field $\mathbf{H}^*_{\mathrm{eff}}$, which is a vector sum of $\mathbf{H}_{\mathrm{eff}}$ and laser-induced field $\mathbf{H}'$ (where $\mathbf{H}'$ denotes$\mathbf{H}^{\mathrm{IFE}}$ for IFE or $\mathbf{H}^{\mathrm{OOE}}$ for OOE). This distinction is central to evaluating their individual contributions.

Possible mechanisms of the optical orientation effect in EuO were discussed in Ref. [33]. In EuO, optical absorption results from $4f$-to-$5d$ transitions: $4f^7(^8\mathrm{S}_{7/2})5d^0 \rightarrow 4f^6(^7\mathrm{F}_J)5d^1(\mathrm{t}_{2g})$ [34]. Analysis of the

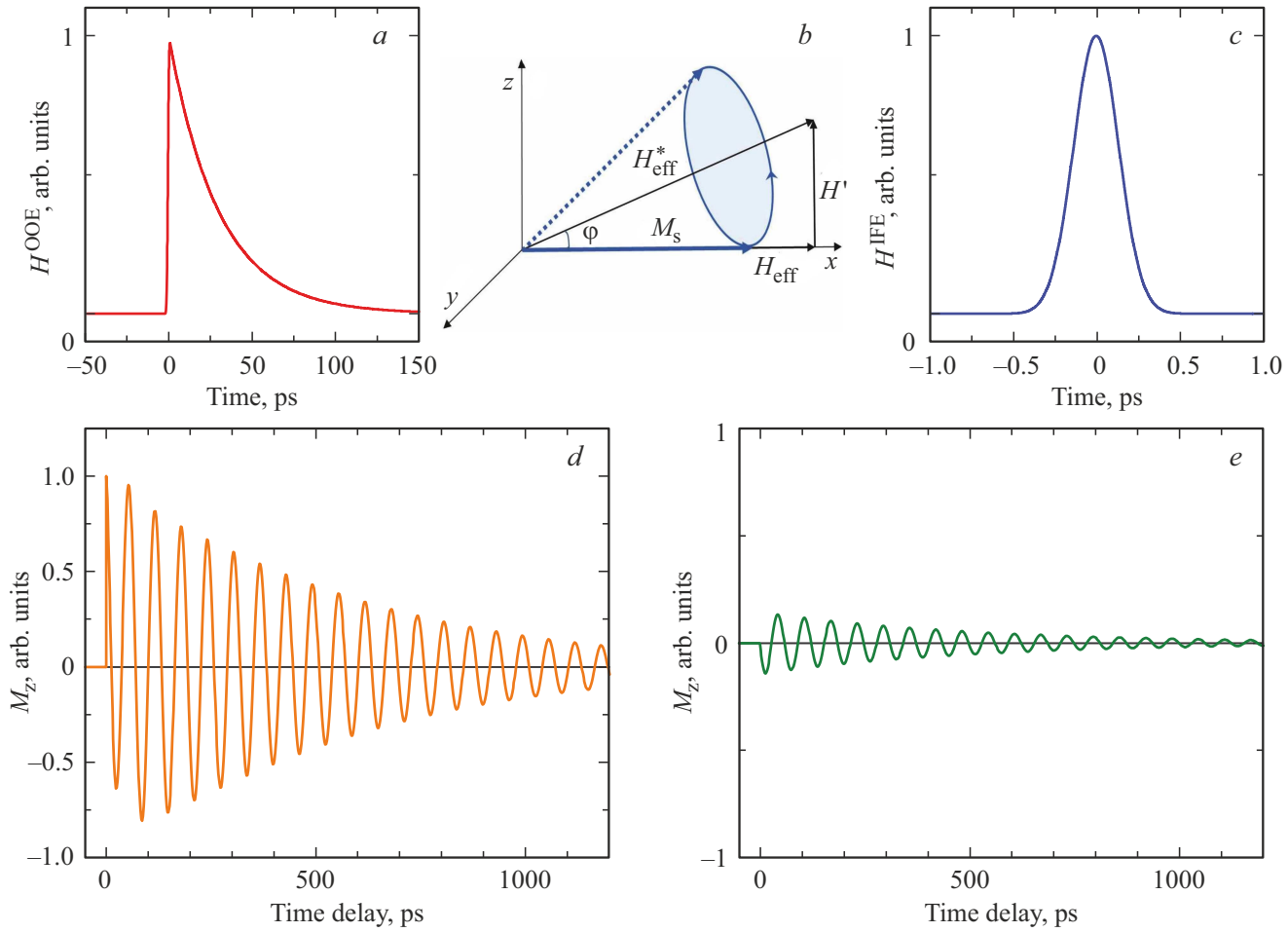

Figure 5. (*a*) Time dependence of the effective magnetic field induced by the OOE $\mathbf{H}^{OOE}$. (*b*) Onset of magnetization $\mathbf{M}_s$ precession driven by the effective magnetic field $\mathbf{H}^*_{eff}$, which results from the combination of the optically generated field $\mathbf{H}'$ and the existing field. (*c*) Time dependence of the effective magnetic field $\mathbf{H}^{IFE}$ induced by IFE. (*d*) Time dependence of the z-component of magnetization due to the optical orientation effect. (*e*) Time dependence of the z-component of magnetization due to the inverse Faraday effect.

selection rules for this process has shown that the optical transition probability depends on both the polarization of the absorbed light and the electron spin orientation in the initial and final states [35]. Analysis of the $4f^7 5d^0 \rightarrow 4f^6 5d^1$ electronic transition in EuO must account for crystal field splitting, exchange splitting, spin-orbit coupling, and the Zeeman effect in the magnetic field [29,36,37]. Despite the complexity of the electron structure of EuO, the multi-electron matrix element for the $4f^7 5d^0 \rightarrow 4f^6 5d^1$ transition is equivalent to the single-electron matrix element [38] and formally corresponds to the atomic $4f_\uparrow \rightarrow 5d_\uparrow$ transition [36]. Figure 6 shows a diagram for the $4f_\uparrow \rightarrow 5d_\uparrow$ transition incorporating the sign of the circular light polarization.

The photoinduced magnetization $\mathbf{M}^{OOE}$ in EuO generated via OOE is given by a tractable expression [20]:

$$M^{OOE} = \frac{c\epsilon_0 g\sqrt{J(J+1)}\mu_B t_p}{nl\hbar\omega}\left(1 - e^{-\kappa l}\right)E^2, \qquad (6)$$

where c is the speed of light in vacuum, ϵ_0 is the electric constant, g is the electron g-factor, J is the total

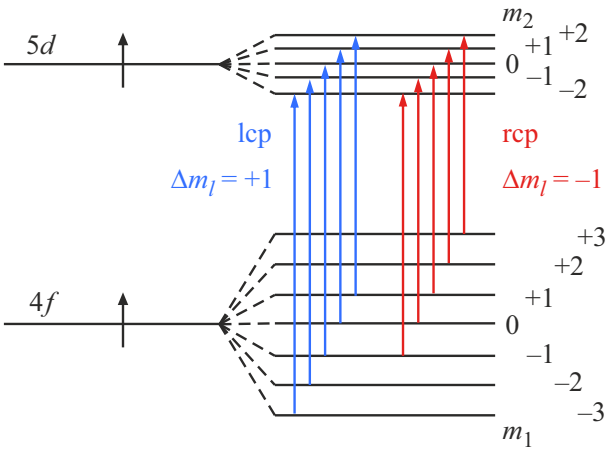

Figure 6. Diagram of the atomic electronic transition $4f_\uparrow \rightarrow 5d_\uparrow$ excited by circularly polarized light, showing selection rules $\Delta m_l = +1$ for left (lcp) and -1 for right circular polarization (rcp), respectively [36,38].

Physical parameters of the EuO sample required for estimating IFE and OOE

Quantity	Symbol	Value	SI unit
Sample thickness	l	$1 \cdot 10^{-7}$	m
Dielectric permittivity	$\epsilon_1 + i\epsilon_2$	$2.5 + i1.1$	
Refractive index	n	1.6	
Absorption coefficient	κ	$7.5 \cdot 10^6$	1/m
Saturation magnetization	M_S	$1.9 \cdot 10^6$	A/m
Magnitude of the gyration vector	G	0.076	

angular momentum of the $5d^1$-electron, n is the refractive index, κ is the absorption coefficient of EuO, l is the sample thickness, $\hbar\omega$ is the photon energy, μ_B is the Bohr magneton, and E is the electric field of the electromagnetic wave. The OOE response in EuO to pump laser pulse excitation can be modeled as a simple exponential decay:

$$A(t) = A_0 \exp\left(-\frac{t}{\tau_s}\right), \tag{7}$$

where τ_s denotes the spin relaxation time. The decaying function models both the photoinduced magnetization M^{OOE} and the resulting Weiss field $H^{\mathrm{OOE}} = A(t)\lambda M^{\mathrm{OOE}}/\mu_0$ (see Figure 5, *a*), which share identical temporal dynamics and drive the f-electron system. The Weiss field acts on the f-electron system via strong exchange interaction (integral $J^{\mathrm{df}} \sim 0.1\,\mathrm{eV}$ [37,39]) between the excited $5d^1$-electron and $4f$-electrons of Eu^{2+} with parameter λ [40,41]. In other words, the magnetic field H^{OOE} acts on the $4f$-electron during the spin lifetime (i. e., the spin relaxation time τ_s) of excited $5d$-electrons.

We performed theoretical modeling by numerically solving the Landau-Lifshitz equation (1). The solution requires the time-dependent effective field $\mathbf{H}^*_{\mathrm{eff}}$, which was computed as either the OOE-induced field (using Eqs. (6) and (7), see Figure 5, *a*) or the IFE-induced field (using Eqs. (4) and (5), see Figure 5, *c*). Our evaluation of the OOE- and IFE-induced z-component of magnetization was based on the physical parameters of the EuO sample given in the table. The modeling, employing the distinct effective fields of OOE and IFE, directly reveals their differing impacts on the system's dynamics: the calculated time evolution of the z-component of the magnetic moment of the system of f-electrons is shown for OOE in Figure 5, *d* and for IFE in Figure 5, *e*. The calculations reveal a substantial disparity between the two mechanisms: for a 200 mT field, the amplitude ratio is $M_z^{OOE}/M_z^{IFE} \sim 40$, demonstrating the overwhelming contribution of OOE at the selected wavelength. Furthermore, the simulations uncover a fundamental distinction in the initial precession phase — cosinusoidal for OOE versus sinusoidal for IFE. This phase difference, along with the accurate reproduction by the OOE model of the experimental magnetization dynamics (see Figure 4, *a*), provides compelling evidence that the optical orientation effect is the dominant mechanism responsible for triggering magnetization precession in EuO films.

A key advantage of our experimental approach is the use of transmission geometry, further enhanced by modulating the pump polarization. Unlike the reflection geometry with fixed polarization employed in Ref. [20], our method isolates the magnetic response specifically to the pump helicity reversal. This provides direct access to the volumetric properties of the EuO films, enabling a more accurate assessment of the parameters crucial for laser-induced magnetization precession. Fitting the theoretical model to the experimental data yields the magnetization damping rate α and the spin relaxation time τ_s of the excited $5d$-electrons. For this purpose, the measurement results obtained in a magnetic field with an induction of 200 mT can be used. The analysis yielded a magnetization relaxation rate of $\alpha \sim 0.02$ and a spin lifetime τ_s. The spin lifetime, i. e., the time during which the spins of the photoexcited $5d$-electrons retain their net orientation, was determined to be ~ 30 ps. This value agrees well with the literature data for other europium chalcogenides, such as EuTe and EuSe, where the spin lifetime is also on the order of tens of picoseconds [42,43]. The Weiss field from OOE is considerably longer-lived ($\propto \tau_s$) than its IFE counterpart, which is limited to the laser pulse duration ($\propto \varrho$). This establishes OOE as the dominant mechanism for triggering magnetization precession in EuO films with femtosecond laser pulses, confirming the conclusion reached in Ref. [20].

4. Dynamics of Photoinduced Magnetic Polarons

This section examines the dynamics of the photoinduced Faraday effect (PFE) in EuO across time scales from picoseconds to microseconds at temperatures slightly above the Curie temperature $T_{\mathrm{C}} = 69.8\,\mathrm{K}$, drawing on data from Ref. [15]. The experimental geometry here features an external magnetic field applied perpendicular to the sample plane. For ferromagnetic materials, the Faraday effect accounting for photoinduced magnetization can be expressed

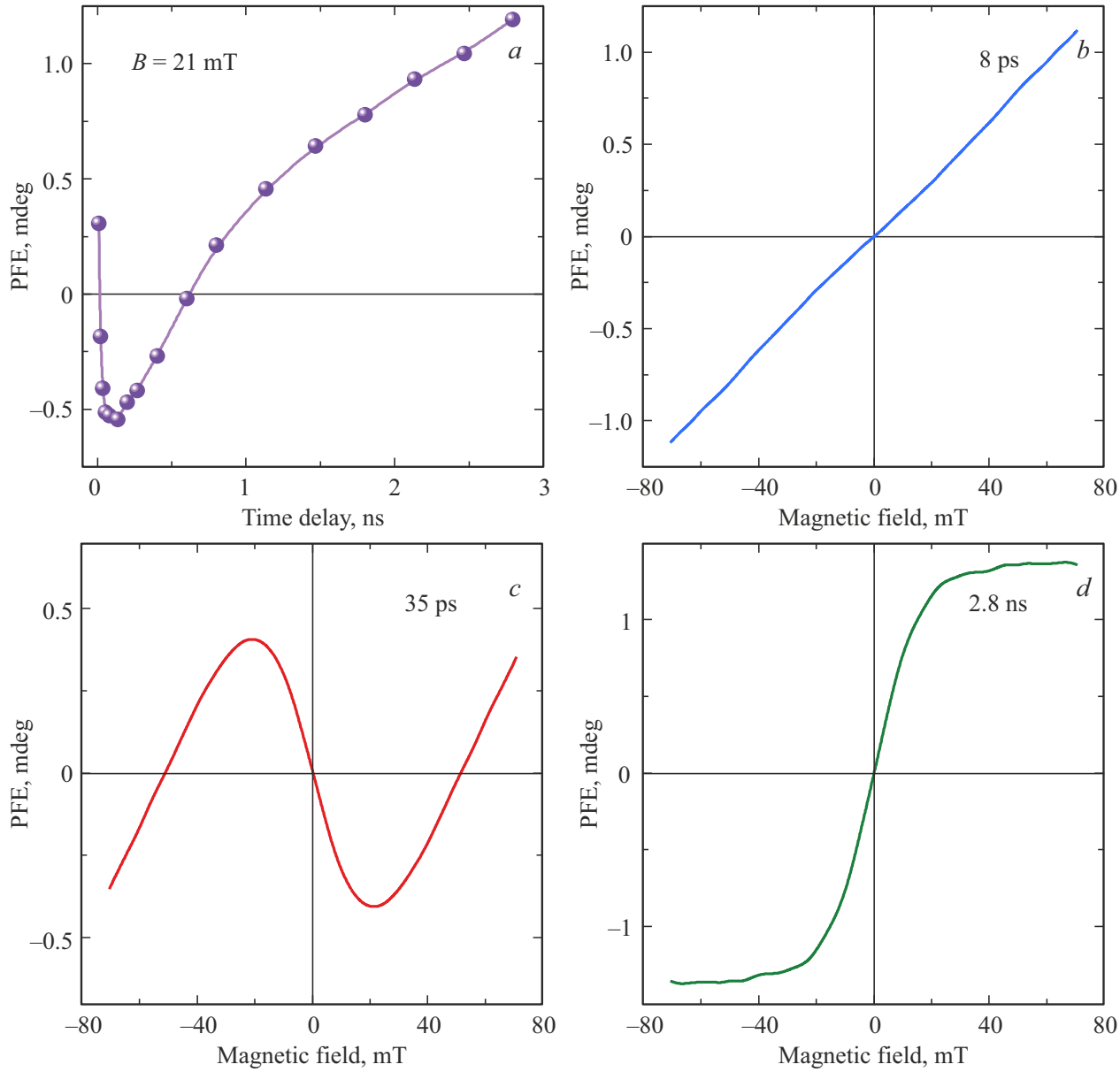

Figure 7. (a) Time-resolved dynamics of the photoinduced Faraday effect (PFE). Experimental data are shown by dots, the line represents a spline approximation; (b), (c), (d) Magnetic field dependence of the PFE at different time delays. The experimental data were acquired at $T = 70.8$ K (from Ref. [15].

)

as follows:

$$\Theta_F = V[M_s + M_{ph}(I)]l, \qquad (8)$$

where V — Verdet constant, M_{ph} — photoinduced magnetization, I — pump intensity. The spontaneous magnetization term M_s gives the conventional Faraday effect, and the photoinduced magnetization term M_{ph} represents the PFE contribution.

The temporal evolution of the PFE with pump-probe delay is shown in Figure 7, a. Figures 7, b–d complement this by showing the evolution of the PFE's magnetic field dependence at specific delay times. It is important to note that the shape of the PFE dependence on the magnetic field undergoes a pronounced evolution. Thus, at a short delay time of 8 ps the PFE displays an almost linear dependence on the external magnetic field B. At time delay of 35 ps, the PFE versus B dependence reveals behavior that can be described as a sum of a linear function and a negative S-type dependence. At a delay of 2.8 ns the PFE versus B dependence takes the form of a positive S-type curve.

The appearance of an S-shaped PFE(B) dependences at long delays indicates that, slightly above the Curie temperature, the PFE originates from the formation and dynamics of photoinduced magnetic polarons (MP) in EuO. This leads us to examine the formation mechanism of photoinduced

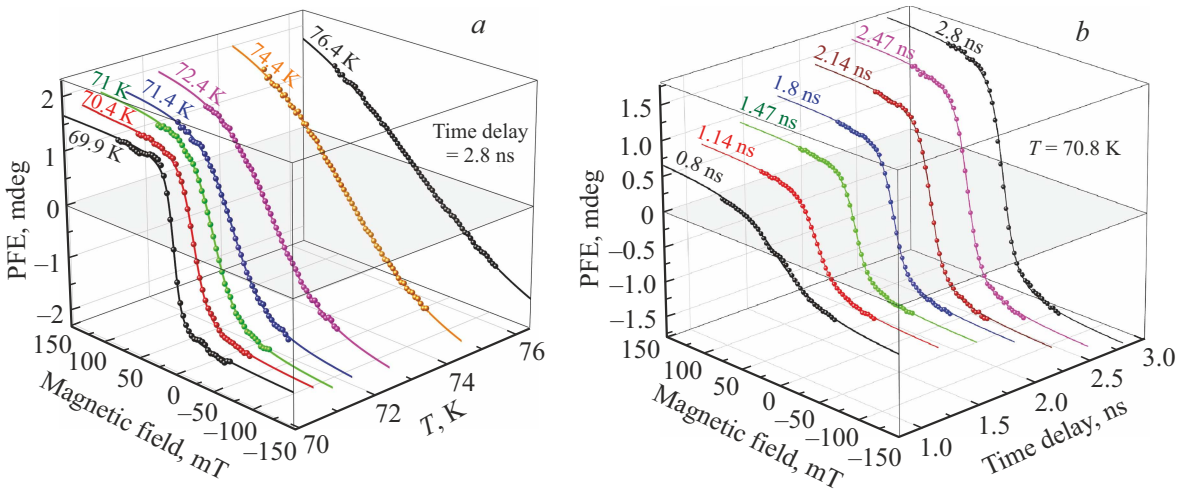

Figure 8. (*a*) Magnetic field dependence of the PFE at different temperatures and a fixed time delay of 2.8 ns. (*b*) Magnetic field dependence of the PFE at different time delays and a fixed temperature of $T = 70.8$ K.

MP, which originates from the $4f^7 5d^0 \rightarrow 4f^6 5d^1$ electronic transition and involves the subsequent relaxation processes within the EuO conduction band. The complete Hamiltonian describing the charge carriers and magnetic moments in EuO is given by the sum of several components [44,45]:

$$H = H_{\mathrm{k}} + H_{\mathrm{C}} + H_{\mathrm{ff}} + H_{\mathrm{df}}, \tag{9}$$

where H_{k} is the kinetic energy operator of the band electrons, H_{C} the Coulomb energy operator of a photo-excited electron-hole pair, H_{ff} the Heisenberg Hamiltonian for the magnetic lattice of f-electron spins, and H_{df} describes the exchange interaction between the spin of $5d^1$-electron in the conduction band and the localized f-electron spins. The Hamiltonian H_{ff} involves two exchange integrals — $J_1 \sim 0.09$ meV and $J_2 \sim 0.01$ meV [45] — that are responsible for the ferromagnetic ordering of the f-electron spins in EuO. For a $5d^1$ electron which is Coulomb-bound to a $4f^6$ hole and whose wavefunction overlaps n Eu^{2+} ions, the exchange energy may be written as follows [46]

$$H_{\mathrm{df}} = -2\sum_{i}^{n} \frac{J^{\mathrm{df}}}{n} \mathbf{s} \cdot \mathbf{S}_i, \tag{10}$$

where $\mathbf{s}$ is the spin operator of the $5d^1$-electron, and $\mathbf{S}_i$ is the total spin operator of the $4f$-electrons of the i-th Eu^{2+} ion. The strong coupling mediated by H_{df} between electrons in the $5d$ conduction and $4f$ valence bands is decisive for MP formation in europium chalcogenides [45,47].

In EuO the laser pulse with an intensity of 0.5 mJ/cm^2 creates an electron concentration $\sim 10^{17}$ cm^{-3} in the conduction band. In the case of non-interacting electrons at low concentration with random spin alignment, the magnetization follows this expression: [48]:

$$m_z = M_0 B_J(x). \tag{11}$$

where: M_0 is the saturation magnetization, $B_J(x)$ the Brillouin function, J is the total angular momentum, and $x = m_0 B_z / k_B T$ the dimensionless magnetic-to-thermal energy ratio, with $m_0 = g\mu_B J$ the magnetic moment of an individual electron, B_z the z-component of the external magnetic field, k_B Boltzmann constant, and T the temperature. The magnetic moment grows significantly during the polaron formation process. The isolated polarons with random moment orientations are commonly described as a superparamagnetic system, with magnetization approximated by [48]:

$$m_z = M_0 L(x). \tag{12}$$

where $L(x) = \coth(x) - \frac{1}{x}$ is the Langevin function, with $x = \mu_{pol} B_z / k_B T$, and μ_{pol} is the magnetic moment of an individual polaron.

Presented in Figure 8, *a* are the PFE versus magnetic field dependences for EuO measured across temperatures of 70–76.4 K, just above the Curie point. Figure 8, *b* presents a series of PFE versus magnetic field curves acquired at different time delays, revealing systematic changes in the lineshape evolution with increasing delay. The magnetic field dependences of PFE show an approximately *S*-shaped behavior, qualitatively matching the Langevin function. Based on this correspondence, we determine the polaron magnetic moment by applying equation (12), with additional terms for the linear contribution including that from equation (11), and demagnetization factor of EuO film [15]. The experimental results (points in Figure 8) show close correspondence with the calculated curves (lines), confirming the model's validity. The maximum magnetic moment of the polarons, determined to be $175 \cdot 10^3 \mu_B$, was detected at $T = 70$ K with 2.8 ns delay and, additionally, in the 0.3–0.4 ns temporal window at $T = 70.8$ K [15].

Figure 9, *a* shows the optical excitation process from the $4f$ valence band ground state to the $5d$ conduction band excited state in EuO, where magnetic polaron formation begins. An excited $5d^1$-electron, interacting with $4f$-electrons through an exchange integral J^{df}, constitutes the

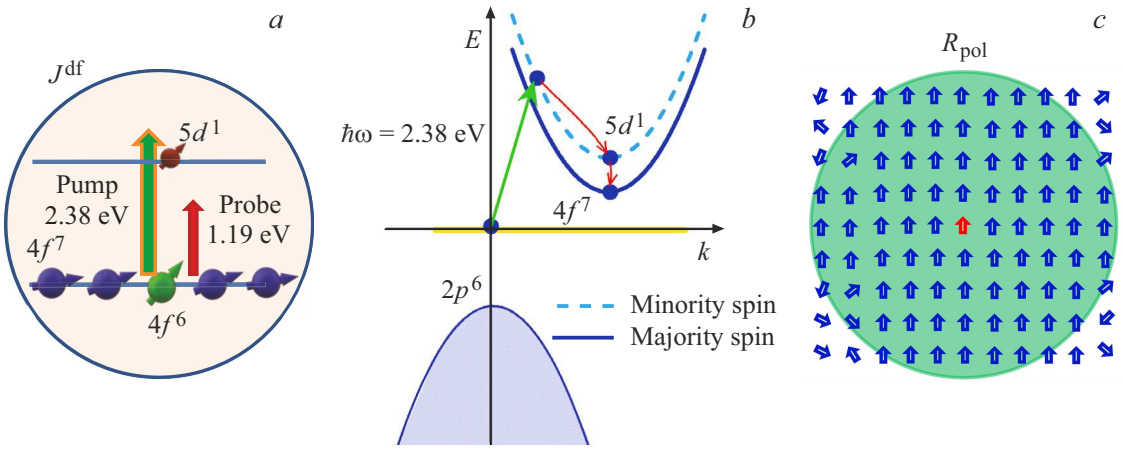

Figure 9. (*a*) Diagram of the $4f^7 5d^0 \rightarrow 4f^6 5d^1$ electronic transition in EuO for pump-probe experiments. (*b*) Optical excitation in the *E*-*k* diagram, corresponding to electron transfer from the $4f$ valence band to $5d$ conduction band, followed by sequential relaxation into $\downarrow$ and $\uparrow$ subbands. (*c*) Magnetic polaron with radius R_{pol}, formed by an excited $5d^1$-electron; the red arrow indicates the spin of Eu^{2+} ion's $5d^1$ electron , blue arrows show the $4f$-electron spins.

MP. Within this model [45], the excited $5d^1$-electron creates perfect ferromagnetic alignment inside the MP. Based on the magnetic moment per Eu^{2+} ion ($7\mu_B$) [49], the MP radius in EuO can be evaluated. From this maximum moment $\mu_{pol} \sim 175 \cdot 10^3 \mu_B$, we derive an MP radius of approximately 11 lattice parameters, considering the four Eu^{2+} ions per unit cell [15]. The theory of photoinduced MPs in europium chalcogenides predicts magnetic moments as high as several tens of thousands of Bohr magnetons for EuO [41]. According to this theoretical framework, the MP magnetic moment should exhibit a sharp peak near the Curie temperature. Two qualitatively distinct stable energy states are possible for polarons in ferromagnetic semiconductors [50]. In the first scenario, the charge carrier is delocalized over thousands of unit cells, which is necessary for forming large-radius photoinduced spin polarons with giant magnetic moments. In the second scenario, the carrier is localized to a minimal size, down to a single unit cell. This results in small-radius polarons that escape detection by our method. As temperature increases through $T > T_C$, large-radius polarons collapse into small-radius ones [51]. This behavior is qualitatively consistent with the evolution of the PFE vs B lineshape across temperatures, compatible with the collapse of large polarons. A narrow maximum in the photoinduced response is also found in both europium sulfide (EuS) films (PFE) [52] and bulk EuS (photoinduced Kerr effect) [53] near their Curie temperature.

Ref. [15] presents an experimental study of the polaron magnetic moment dynamics over time. Polaron formation occurs on a timescale of several hundred picoseconds. Let us now discuss the temporal hierarchy of different processes during photoinduced MP formation (see Figure 9, *b*). Following photoexcitation, the $5d^1$-electrons begin to relax, populating the upper energy minimum of the $\downarrow$ spin subband. These electrons commence MP formation within a time interval of 0–0.2 ns. The resulting PFE signal comprises a sum of two contributions: a linear Brillouin function term for electrons that have not yet formed MPs, and a negative, *S*-type Langevin function dependence for those electrons that have formed MPs (see Figure 9, *c*). During subsequent relaxation within the 0.2–1 ns time window, the electrons may reach the lower energy minimum of the $\uparrow$ spin subband, which corresponds to spins aligned with the applied magnetic field B. Experimentally, this manifests as a smooth transition in the PFE(B) dependence from negative to positive *S*-shaped behavior — effectively, a reversal of the hysteresis loop. The MP magnetic moment increases linearly, reaching $175 \cdot 10^3 \mu_B$ at 0.3 ns, then decreases to $90 \cdot 10^3 \mu_B$ by 1 ns, as the $5d^1$ electrons relax into the lower minimum corresponding to the $\uparrow$ spin state. The MP moment subsequently stabilizes at $90 \cdot 10^3 \mu_B$ within the 1–2.8 ns time window. Within the superparamagnetic picture of randomly oriented polarons, the PFE is understood to scale with the product of polaron density and moment, explaining its increase with delay time. Complementing this picture of polaron density evolution, the PFE relaxation time in EuO — equivalent to the polaron lifetime — was found to be 5 μs [15]. This lifetime agrees well with those measured for other europium chalcogenides: 1.6 μs in EuSe [54], 13 μs in EuS [53], and 15 μs in EuTe [43].

5. Conclusion

Our findings, summarized in this mini-review, demonstrate that pump-probe measurements are a powerful tool for unraveling the photoinduced magnetic state dynamics in thin epitaxial EuO films. By employing our advanced approach with polarization modulation in transmission geometry, we have firmly established the optical orientation effect (OOE) as the mechanism triggering magnetization

precession at temperatures well below the Curie point, thereby providing more robust confirmation of the conclusion in Ref. [20]. The underlying mechanism involves the optical orientation of spins via the $4f^7 5d^0 \rightarrow 4f^6 5d^1$ electronic transition upon excitation with circularly polarized laser pulses. The resulting spin polarization, through strong exchange interaction, generates an effective Weiss field that acts on the magnetic moment of the f-electron system, giving rise to a photoinduced magnetization. The faithful reproduction of the experimental data by the theoretical model allowed us to both quantify the individual contributions, showing that the OOE surpasses the IFE by a factor of 40, and extract key parameters such as the magnetization damping rate and the spin relaxation time. The origin of the OOE dominance lies in the substantially longer duration of its induced Weiss field, which persists over the spin relaxation time, compared to the IFE-generated field, which is confined solely to the ultrafast laser pulse duration.

Above T_C, the response of EuO to above-bandgap light is consistent with a superparamagnetic ensemble of magnetic polarons, which we observe to have a lifetime of $5\,\mu$s and a giant magnetic moment — up to $175 \cdot 10^3 \mu_B$ — that sets a record among known materials [15]. The dynamics of these polarons span a range from picoseconds to microseconds and display a complex relaxation pattern, which is associated with the sequential relaxation of the electron within the conduction band. The initial stage (first $0-0.2$ ns) features dynamics that can be interpreted within a model where a superparamagnetic polaron ensemble forms around photoexcited $5d$-electrons in the upper energy minimum of the $\downarrow$ spin subband. Subsequently, within the $0.2-1$ ns time window, a reversal of the PFE hysteresis loop is observed, which we interpret as a consequence of the photoexcited electrons relaxing into the lower energy minimum of the $\uparrow$ spin subband.

The mechanisms of spin order control in EuO uncovered in this work represent a novel approach in optomagnetism and hold promise for practical applications in spintronic and optoelectronic devices.

Acknowledgments

The authors express their gratitude to the group of V.G. Storchak (National Research Center, „Kurchatov Institute“, Moscow) for fruitful cooperation.

Funding

This study was supported by the Russian Science Foundation (grant No. 24-12-00348).

Conflict of interest

The authors declare that they have no conflict of interest.

Note on the Translation

The authors have thoroughly reviewed and scientifically edited the English version of this manuscript to ensure the accuracy of the scientific terminology and the clarity of the presentation.

References

[1] A.V. Kimel, A.M. Kalashnikova, A. Pogrebna, A.K. Zvezdin. Phys. Rep. **852**, 1 (2020).
[2] A. El-Ghazaly, J. Gorchon, R.B. Wilson, A. Pattabi. J. Bokor. J. Magn. Magn. Mater. **502**, 166478 (2020).
[3] L.P. Pitaevskij. Sov. Phys. JETP, **12**, 1008 (1961).
[4] A.V. Kimel, A. Kirilyuk, P.A. Usachev, R.V. Pisarev, A.M. Balbashov, Th. Rasing. Nature **435**, 655 (2005).
[5] A. Kirilyuk, A.V. Kimel, Th. Rasing. Rev. Mod. Phys. **82**, 2731 (2010).
[6] P.S. Pershan, J.P. van der Ziel, L.D. Malmstrom. Phys. Rev. **143**, 574 (1966).
[7] A.H.M. Reid, A.V. Kimel, A. Kirilyuk, J.F. Gregg, Th. Rasing. Phys. Rev. Lett. **105**, 107402 (2010).
[8] D. Popova, A. Bringer, S. Blügel. Phys. Rev. B **85**, 094419 (2012).
[9] F. Hansteen, A. Kimel, A. Kirilyuk, Th. Rasing. Phys. Rev. B **73**, 014421 (2006).
[10] L.A. Shelukhin, V.V. Pavlov, P.A. Usachev, P.Yu. Shamray, R.V. Pisarev, A.M. Kalashnikova. Phys. Rev. B **97**, 014422 (2018).
[11] E. Beaurepaire, J.-C. Merle, A. Daunois, J.-Y. Bigot. Phys. Rev. Lett. **76**, 4250 (1996).
[12] F. Meyer, B.P. Zakharchenya (Eds.). Optical orientation, North Holland, Amsterdam, (1984), 523 p.
[13] A. Kastler. J. Phys. Radium **11**, 255 (1950).
[14] P. Němec, E. Rozkotová, N. Tesarová, F. Trojánek, E. De Ranieri, K. Olejník, J. Zemen, V. Novák, M. Cukr, P. Malý, T. Jungwirth. Nat. Phys. **8**, 411 (2012).
[15] P.A. Usachev, V.N. Kats, L.A. Shelukhin, V.V. Pavlov, D.V. Averyanov, I.S. Sokolov, O.E. Parfenov, O.A. Kondratev, A.N. Taldenkov, A.V. Inyushkin, A.M. Tokmachev, V.G. Storchak. Mater. Horiz. **12**, 512 (2025).
[16] V.N. Kats, S.G. Nefedov, L.A. Shelukhin, P.A. Usachev, D.V. Averyanov, I.A. Karateev, O.E. Parfenov, A.N. Taldenkov, A.M. Tokmachev, V.G. Storchak, V.V. Pavlov. Appl. Mater. Today **19**, 100640 (2020).
[17] J.C. Suits, K. Lee. J. Appl. Phys. **42**, 3258 (1971).
[18] M. Matsubara, A. Schroer, A. Schmehl, A. Melville, C. Becher, M. Trujillo-Martinez, D.G. Schlom, J. Mannhart, J. Kroha, M. Fiebig. Nat. Commun. **6**, 6724 (2015).
[19] F. Formisano, R. Medapalli, Y. Xiao, H. Ren, E.E. Fullerton, A.V. Kimel. J. Magn. Magn. Mater. **502**, 166479 (2020).
[20] V.N. Kats, L.A. Shelukhin, P.A. Usachev, D.V. Averyanov, I.A. Karateev, O.E. Parfenov, A.N. Taldenkov, A.M. Tokmachev, V.G. Storchak, V.V. Pavlov. Nanoscale **15**, 2828 (2023).
[21] V. Goian, R. Held, E. Bousquet, Y. Yuan, A. Melville, H. Zhou, V. Gopalan, P. Ghosez, N.A. Spaldin, D.G. Schlom, S. Kamba. Commun. Mater. **1**, 74 (2020).
[22] S. Sugahara, M. Tanaka. US patent US7671433B2 (2010).
[23] L.D. Landau, E.M. Lifshits. Phys. Z. Sowjet. **8**, 153 (1935).
[24] G.V. Skrotskij. Physics — Uspekhi **27**, *12*, 977 (1984).
[25] M. Farle. Rep. Prog. Phys. **61**, 755 (1998).

[26] R.S. Hughes, G.E. Everett, A.W. Lawson. Phys. Rev. B **9**, 2394 (1974).
[27] Y.R. Shen. The principles of nonlinear optics, Wiley-Interscience, New York, (1984).
[28] M.A. Kozhaev, A.I. Chernov, D.A. Sylgacheva, A.N. Shaposhnikov, A.R. Prokopov, V.N. Berzhansky, A.K. Zvezdin, V.I. Belotelov. Sci. Rep. **8**, 11435 (2018).
[29] J. Schoenes. J. Magn. Soc. Jpn. **11** (Suppl. S1), 99 (1987).
[30] G. Güntherodt. Phys. Condens. Matter **18**, 37 (1974).
[31] A.K. Zvezdin, V.A. Kotov. Modern magnetooptics and magnetooptical materials. CRC Press, Boca Raton, (1997).
[32] J.P. van der Ziel, P.S. Pershan, L.D. Malmstrom. Phys. Rev. Lett. **15**, 190 (1965).
[33] M.M. Afanas'ev, M.E. Kompan, I.A. Merkulov. Sov. Phys. JETP **44**, 1086 (1976).
[34] P. Wachter. Phys. Kond. Mater. **8**, 80 (1968).
[35] J.O. Dimmock, J. Hanus, J. Feinleib. J. Appl. Phys. **41**, 1088 (1970).
[36] P. Fumagalli, J. Schoenes. Magneto-optics: an introduction, De Gruyter, Berlin, Boston, (2021).
[37] T. Kasuya. CRC Critical Reviews on Solid State Sciences **3**, 131 (1972).
[38] A.B. Henriques, M.A. Manfrini, P.H.O. Rappl, E. Abramof. Phys. Rev. B **77**, 035204 (2008).
[39] G. Güntherodt. Phys. Cond. Matter **18**, 37 (1974).
[40] S. Blundell. Magnetism in condensed matter, Oxford University Press, Oxford, (2001).
[41] S.C.P. van Kooten, X. Gratens, A.B. Henriques. Phys. Rev. B **103**, 035202 (2021).
[42] V.V. Pavlov, R.V. Pisarev, S.G. Nefedov, I.A. Akimov, D.R. Yakovlev, M. Bayer, A.B. Henriques, P.H.O. Rappl, E. Abramof. J. Appl. Phys. **123**, 193102 (2018).
[43] A.B. Henriques, A.R. Naupa, P.A. Usachev, V.V. Pavlov, P.H.O. Rappl, E. Abramof. Phys. Rev. B **95**, 045205 (2017).
[44] P. Kuivalainen, J. Sinkkonen, T. Stubb. Phys. Stat. Sol. (b) **104**, 299 (1981).
[45] A. Mauger. Phys. Rev. B **27**, 2308 (1983).
[46] J.B. Torrance, M.W. Shafer, T.H. McGuire. Phys. Rev. Lett. **29**, 1168 (1972).
[47] E.L. Nagaev. Phys. Stat. Sol. (b) **145**, 11 (1988).
[48] J.M.D. Coey. Magnetism and magnetic materials, Cambridge University Press, Cambridge, (2009).
[49] P. Wachter. Europium chalcogenides: EuO, EuS, EuSe and EuTe, in Handbook on the physics and chemistry of rare earths, K.A. Gschneider, L.R. Eyring (Eds.), North-Holland, Amsterdam, (1979), P. 507.
[50] D. Emin. Polarons, Cambridge University Press, (2012).
[51] D. Emin. Mat. Res. Soc. Symp. Proc. **494**, 163 (1998).
[52] X. Gratens, Y. Ou, J.S. Moodera, P.H.O. Rappl, A.B. Henriques. Appl. Phys. Lett. **116**, 152402 (2020).
[53] P.A. Usachev, V.N. Kats, V.V. Pavlov. Phys. Solid State, **62**, *9*, 1619 (2020).
[54] A.B. Henriques, X. Gratens, P.A. Usachev, V.A. Chitta, G. Springholz. Phys. Rev. Lett. **120**, 217203 (2018).

Translated by E.Ilinskaya